

Representation Learning of Point Cloud Upsampling in Global and Local Inputs

Tongxu Zhang^{a,b}, Bei Wang^a

^a*East China University of Science and Technology, 130 Meilong Road, Shanghai, 200237, Shanghai, China*

^b*The Hong Kong Polytechnic University, Hung Hom, Kowloon, Hong Kong, , Hong Kong SAR, China, Hong Kong*

Abstract

In recent years, point cloud upsampling has been widely applied in fields such as 3D reconstruction. Our study investigates the factors influencing point cloud upsampling on both global and local levels through representation learning. Specifically, the paper inputs global and local information of the same point cloud model object into two encoders to extract these features, fuses them, and then feeds the combined features into an upsampling decoder. The goal is to address issues of sparsity and noise in point clouds by leveraging prior knowledge from both global and local inputs. And the proposed framework can be applied to any state-of-the-art point cloud upsampling neural network. Experiments were conducted on a series of autoencoder-based models utilizing deep learning, yielding interpretability for both global and local inputs, and it has been proven in the results that our proposed framework can further improve the upsampling effect in previous SOTA works. At the same time, the Saliency Map reflects the differences between global and local feature inputs, as well as the effectiveness of training with both inputs in parallel.

Keywords: Deep learning, Point cloud, Upsampling, Feature extract, Interpretability

1. Introduction

LiDAR and depth cameras have seen widespread use due to advancements in 3D sensors and 3D scanners, mostly relying on point clouds to collect data. However, issues such as sparsity, uneven distribution, noise, and redundancy

are common in current point cloud data collection. Due to unavoidable flaws in point cloud data collection, such as occlusion, generating denser and higher-quality 3D point clouds through point cloud upsampling methods, similar to tasks performed on complete point clouds, is essential. This allows point clouds to fully demonstrate their significant value in 3D reconstruction [1], object detection and classification [2, 3, 4], and robotic operations [5].

The irregular nature of point clouds makes them easy to update [6], as each point in a point cloud is independent, making it convenient to add new points and perform interpolation [7]. However, it is challenging to apply convolution to point clouds when using learning-based methods. Nonetheless, through graph-based methods [8], works such as [9, 10, 11] have facilitated the application of deep learning in point cloud tasks. Subsequently, PU-Net [12] proposed the first deep learning-based upsampling method for point clouds. With the development of Graph Convolution Networks (GCN) [13], models like MPU/3PU [14] have used clustering for interpolation, enabling better local and edge recognition in point clouds. Building on this, PU-GCN [15] further improved feature extraction, constructing DenseGCN for extracting local input features from point clouds, achieving better results. Additionally, PU-GAN [16] applies generative adversarial networks [17], using generators to upsample and produce high-fidelity, realistic point clouds. PU-Transformer [18] further advanced this field by utilizing positional information and self-attention mechanisms for enhanced global feature extraction.

Although significant progress has been made in point cloud upsampling through deep learning [19, 20, 21], substantial challenges remain. As noted, unlike voxel-based grid representations of 3D models [22, 23], each point in a point cloud is independent. Ergo, [24] extracts features from voxels to reduce the problem of inaccurate feature extraction caused by the irregularity and sparsity of point clouds. But, for the point clouds, independence brings unique challenges in extracting objective features of objects, particularly in incomplete or sparse regions with limited information. This is akin to the task of working with incomplete point clouds, where global features are extracted from partial inputs but lose geometric details due to incompleteness [25]. Therefore, effectively aligning local details with global information is crucial. While Zhang [26] has discussed the influence of local and global inputs on point cloud upsampling, it lacks interpretability and breadth in experimental models. Current methods [27, 28, 20] utilize refiners on coarse point clouds to merge local and global features, but their networks, which are single-encoder structures, face limitations in ensuring consistency and precise

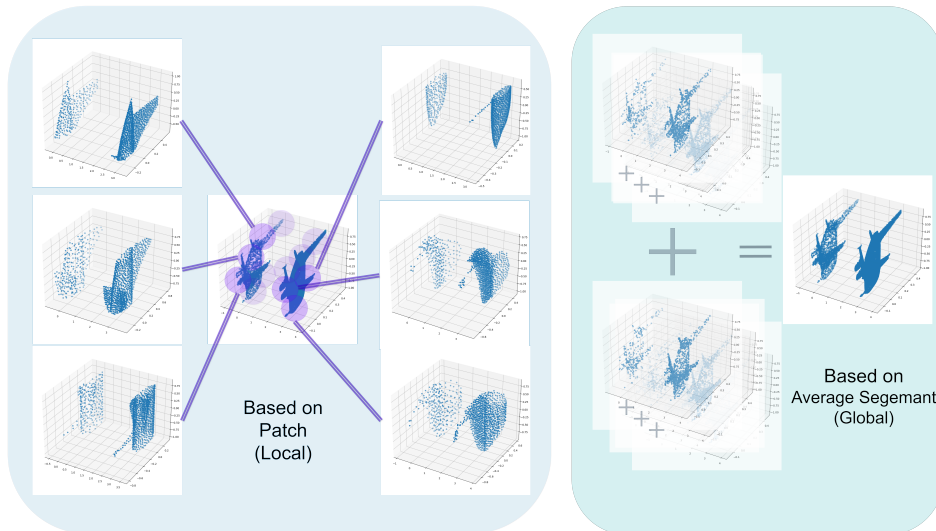


Figure 1: Schematic diagram of two data input methods as the transcendental local and global feature for point cloud upsampling.

alignment of cross-scale features. BiPU [29] employs asymmetric, dedicated encoders for local and global inputs, intending to combine local and global feature information efficiently through parallel extraction. Indeed, upsampling largely relies on local information and knowledgeable global priors. Parallel extraction, similar to that in image domains [30], is necessary, but the need for highly specialized global and local feature extraction remains in question. To avoid complexity in feature extraction within the encoder part, we propose using the same encoder for both global and local features, thus avoiding complex networks.

Therefore, we propose the ReLPU network, adaptable to various encoder-decoder-based point cloud upsampling models. The aim is to address point cloud irregularity and unstructured characteristics by integrating information from both local and global inputs in a parallel decoder. Furthermore, ReLPU enables easy backbone network replacement in future advanced autoencoder-based point cloud upsampling tasks. That is to say, our proposed framework can be used for continuously updating state-of-the-art point cloud upsampling networks. And there is no need for specific specialized network modules to extract local and global features. We validated our method on the publicly available synthetic datasets PU1K [15]. In these experiments, our approach was applied to existing networks and demonstrated superior results

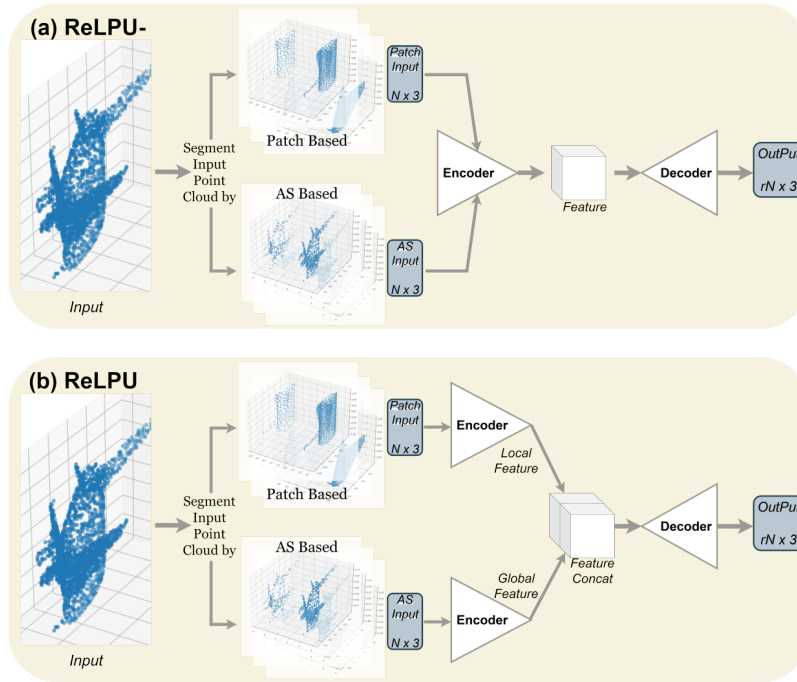


Figure 2: Illustrates the structure of ReLPU- (a) and ReLPU (b) models for point cloud upsampling. ReLPU- uses a sequential autoencoder for unified feature extraction, while ReLPU employs two parallel autoencoders to extract local and global features separately, enhancing upsampling performance.

compared to state-of-the-art methods.

Our main contributions are as follows:

1) We propose the ReLPU network, a new framework for point cloud upsampling with local and global data input encoders. The parallel encoders extract local and global features and can be used in various point cloud upsampling networks based on existing autoencoder architectures.

2) Through representation learning, we calculate gradient contribution values to interpret the local and global inputs, effectively explaining the differences and significance of local and global features in point cloud upsampling.

3) Experiments were conducted on the PU1K datasets, establishing baselines for multiple point cloud upsampling models to demonstrate ReLPU’s superior performance over previous state-of-the-art methods.

2. Related Works

2.1. Deep Learning in Point Cloud Processing

Since PointNet [9, 31], early methods that projected 3D point clouds into multi-view 2D images [32, 33] or converted point clouds into voxel or grid discretizations [23, 34, 35] have gradually shifted toward directly processing point cloud data on a point-based basis. This direct processing approach avoids contextual loss and complex steps involved in data conversion. The mainstream point cloud processing methods have evolved from MLP-based modules starting with PointNet [9] to convolutional neural network-based approaches like PointCNN [36, 37], and most recently, to Transformer [38] based architectures such as Point-Transformer [39]. As observed, transformer-based structures have already been widely explored in point cloud processing.

2.2. Similar Approaches in Point Cloud Completion

Point cloud completion tasks are similar to point cloud upsampling tasks in that they aim to supplement geometric details by extracting global features from partial inputs. With the aid of deep neural networks and extensive 3D datasets, learning-based methods have achieved remarkable performance in shape completion tasks. Similar to point cloud processing, PCN [10] first used a similar encoder to extract features and output dense and completed point clouds from sparse and incomplete inputs. Agrawal et al. [40] employed GAN networks to implement an optimization algorithm for potential noise points. SA-Net [41] used self-attention mechanisms to effectively leverage local structural details. Zhang et al. [25] proposed a feature aggregation strategy to retain essential details. However, these methods only extract global features from partial inputs, leading to information loss during the encoding process. Later, ASFM-Net [7] used parallel global and local feature matching to reasonably infer the missing geometric details of objects.

2.3. Current Developments in Point Cloud Upsampling

Learning-based methods have become prevalent and dominate recent state-of-the-art technology. Specifically, PU-Net [12] was a pioneering work that introduced CNNs into point cloud upsampling based on the PointNet++ [31] backbone. Subsequently, MPU [14] proposed a patch-based upsampling pipeline, allowing flexible upsampling of point cloud patches with rich local details. Additionally, PU-GAN [16] applied a generative model to address the issue of high-resolution point cloud generation. PU-GCN [15] used a

graph-based network structure to achieve effective upsampling performance. Dis-PU [27] employed disentangled refinement units to progressively generate high-quality point clouds from coarse point clouds. PU-EVA [42] introduced an edge-vector-based upsampling approach, similar to Grad-PU [26], to flexibly perform upsampling at different scales. Du et al. (PUCRN) [28] and PU-Transformer [18] optimized point cloud generation and performance through multi-stage structures and Transformer models. However, these methods still face key challenges, especially in sparse or missing regions. The inherent characteristics of point clouds often result in models lacking sufficient information to comprehend and describe these regions, leading to overfitting. We advocate for a symmetric, parallel encoder pair that can replace the above models, with global and local feature input on the data side, shows in Figure 1, to avoid complex networks and ensure interaction between local and global features, thereby preventing information loss in the feature integration process. To validate this information preservation, we use representation learning to visualize gradient contribution values and output a saliency map [43], indicating which points play a critical role in the upsampling process. By using a saliency map to reflect the differences in local and global features between local and global inputs, it indicates that upsampling indeed requires prior knowledge of both local and global features.

3. Methodology

In this paper, we propose a new Representation Learning of Point Cloud (ReLPU) framework and apply it to point cloud upsampling. Specifically, we construct a parallel network for global and local feature extraction based on the two-point cloud data input methods discussed in [26]. In this network, edge attributes are used for detailed geometric patterns, while global attributes aid in a broader understanding of shapes and structures. Finally, we combine geometric features with miscellaneous structural understanding to achieve comprehensive point cloud upsampling. The entire network can be trained in an end-to-end manner. Details are provided in the following sections.

3.1. Network Architecture

Based on this fundamental idea, we employ a sequential autoencoder for point cloud upsampling to extract geometric and miscellaneous structural features, resulting in the ReLPU- model (as shown in Figure 2a). We then

update ReLPU- by using one specific autoencoder to extract geometric features and another identical autoencoder to extract other global features, resulting in the ReLPU model (as shown in Figure 2b). This setup enables ReLPU to perform parallel global and local feature extraction, contrasting with the sequential approach in ReLPU-. ReLPU significantly enhances the upsampling performance of ReLPU-.

For the autoencoder, the backbone network can be replaced based on existing point cloud upsampling models, as long as the model adheres to the encoder (feature extraction) to decoder (feature expansion) structure. In this paper, we use MPU [14], PU-GCN [15], Dis-PU [27], and PUCRN [28] as backbone networks for point cloud feature extraction. This approach aims to validate the effectiveness of our proposed parallel method and to distinguish it from the sequential method. Here, we **concatenate** the global and local features extracted from the feature extraction modules, or encoders, of different networks.

For local input by patch, assuming the entire Model contains M points, divide it into K patches, so we have \mathcal{P}_k as points of patch input. For global input by Average Segment (AS), once sampling is completed, obtain a point set containing M points $\mathcal{P}_{\text{sampled}}$. We hope to divide it into K subsets, each containing M/K points.

The k -th subset is denoted as \mathcal{P}_k , where $k = 1, 2, \dots, K$. Assuming that M can be divided by K , the range of points for each subset is:

$$\mathcal{P}_k = \{p_i \mid (k-1) \cdot \frac{M}{K} + 1 \leq i \leq k \cdot \frac{M}{K}\}$$

After passing through l layers of encoder E , we have:

$$\mathbf{F} = E^{(l)} = \sigma(\mathbf{A}E^{(l-1)}\mathbf{W}^{(l)})$$

where:

- \mathbf{A} is the adjacency matrix.
- $E^{(0)} = \mathbf{X}$, representing the feature matrix of the input point.
- σ is the activation function.

Additionally, let:

- $\mathbf{F}_{\text{global}}$ represent the global feature vector extracted by the autoencoder.

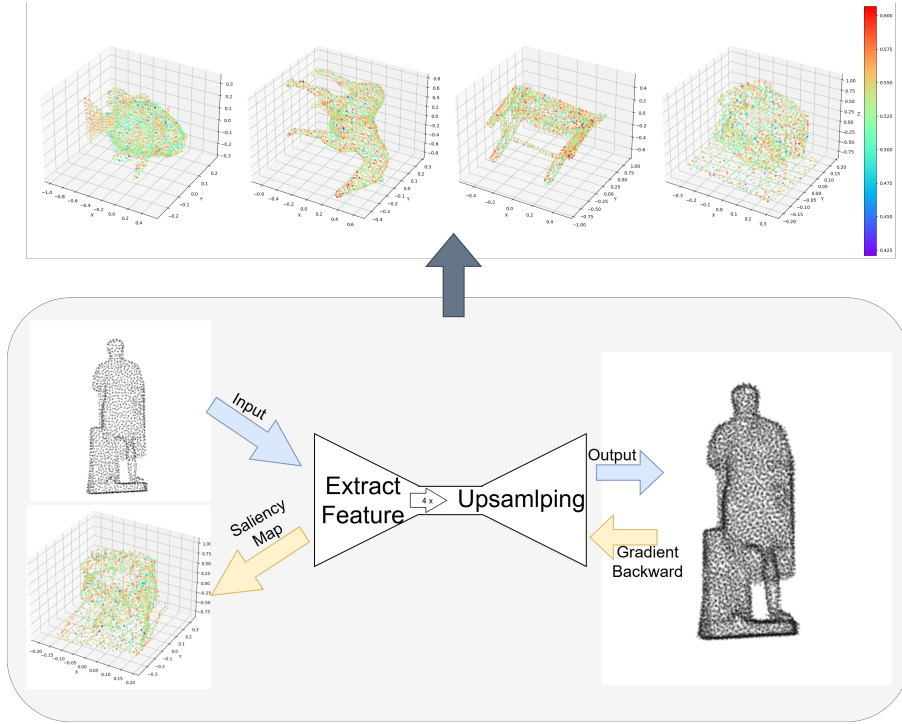


Figure 3: Examples of saliency maps return score-rankings after upsampling in Input.

- $\mathbf{F}_{\text{local}}$ represent the local feature vector extracted by the autoencoder.
- $\mathbf{F}_{\text{concat}}$ represent the concatenated feature vector.

To express this concatenation operation, we can define it as follows:

$$\mathbf{F}_{\text{concat}} = \text{Concat}(\mathbf{F}_{\text{global}}, \mathbf{F}_{\text{local}}) = [\mathbf{F}_{\text{global}}, \mathbf{F}_{\text{local}}] \in \mathbb{R}^{m \times 2d}$$

3.2. Saliency Map for Point Cloud

Whether or not one considers the interpretability of deep learning as essential, using saliency maps to calculate gradient contribution values for data analysis and visualization is a key aspect of explainable artificial intelligence (XAI). It provides an intuitive representation of the key factors underlying model results. Saliency maps have been widely applied in point cloud tasks, particularly for classification and detection [44, 45, 46]. However, these applications are limited to those tasks. Therefore, to understand the contributions

of global and local features to point cloud upsampling and to compare these contributions between sequential and parallel networks, we use saliency maps to reflect the gradients of point clouds during model training, indicating their contribution to upsampling.

Assuming that the loss function of the upsampling model is defined as L , given a point x_i in the point cloud, its contribution can be defined as the difference in loss before and after removing that point:

$$\Delta L_{x_i} = L(X_{\text{gt}}) - L(X_{\{x_{i_{\text{pred}}}\}})$$

where:

- X_{gt} represents the ground truth point cloud.
- $X_{\{x_{i_{\text{pred}}}\}}$ represents the upsampled point cloud after removing point x_i .

In other words, the contribution of a point x_i in the point cloud equals the difference between the loss $L(X_{\text{gt}})$ of the complete point cloud of ground truth and the loss $L(X_{\{x_{i_{\text{pred}}}\}})$ of the point cloud after upsampling.

If the contribution value ΔL_{x_i} is small, we consider point x_i to have a high contribution to the upsampling process, indicating a more accurate resolution after upsampling. Conversely, if ΔL_{x_i} is large, the contribution of point x_i is considered low.

To represent this in the saliency map, we assign each point x_i a sensitivity score s_i , indicating the contribution level of point x_i .

For the **Saliency Map Expression**, formally, the saliency map can be represented as a function $S_\theta(\cdot)$, where $S_\theta(X)$ takes a point cloud X as input and outputs a vector of length N , with each element corresponding to the sensitivity score of each point in the point cloud:

$$S_\theta(X) = \{s_i \mid i = 1, 2, \dots, N\}$$

where the sensitivity score s_i represents the contribution of point x_i . If s_i is high (positive), it indicates that the point has a large positive contribution to the upsampling model. If s_i is low or negative, it indicates that the point has a smaller or negative contribution to the upsampling model, as illustrated in Figure 3, we present the saliency map in input point cloud and the workflow for getting the saliency map.

And then, represent point cloud saliency map as spherical coordinates. In spherical coordinates, point displacement is considered, where a point

is represented as (r, ψ, ϕ) , with r being the distance from the point to the sphere’s center, and ψ and ϕ being the two angular coordinates relative to the sphere’s center. In this spherical coordinate system, moving a point toward the center by δ will increase the loss L by an amount:

$$-\frac{\partial L}{\partial r} \delta.$$

According to the equivalence ΔL_{x_i} , we measure a point’s contribution with a real-valued score: the negative gradient of L with respect to r :

$$s_i = -\frac{\partial L}{\partial r_i} r_i^{1+\alpha}.$$

Thus, in the rescaled coordinate system, we measure the contribution of point x_i simply by using.

3.3. Training Loss Function

During the training process, our end-to-end network uses Chamfer Distance (CD) as the loss function. CD loss is designed to calculate the average closest point distance between two sets of point clouds, describing the discrepancy between the predicted and actual upsampled points.

For the parallel network ReLPU, it is implemented by fine-tuning ReLPU to extract both local and global features, with CD loss remaining unchanged.

Given two sets of point clouds \mathbf{P} and \mathbf{Q} , representing the predicted and ground truth point clouds, respectively, the CD Loss can be expressed as follows:

Let

$$\mathbf{P} = \{p_1, p_2, \dots, p_M\} \quad \text{and} \quad \mathbf{Q} = \{q_1, q_2, \dots, q_N\},$$

where p_i and q_j are points in point clouds \mathbf{P} and \mathbf{Q} , respectively. The Chamfer Distance $d_{\text{CD}}(\mathbf{P}, \mathbf{Q})$ is defined as:

$$d_{\text{CD}}(\mathbf{P}, \mathbf{Q}) = \frac{1}{M} \sum_{i=1}^M \min_{j=1, \dots, N} \|p_i - q_j\|^2 + \frac{1}{N} \sum_{j=1}^N \min_{i=1, \dots, M} \|q_j - p_i\|^2.$$

This loss function minimizes the distance between each point in one set and its nearest neighbor in the other set, thus effectively capturing the geometric discrepancy between the predicted upsampled point cloud and the ground truth.

4. Experiments

4.1. Settings

4.1.1. Dataset

In our study, we conducted experimental validation on two different datasets: a synthetic dataset for training and a real-world object dataset for evaluation. For training and testing the upsampling network, we used the synthetic dataset PU1K [15], which includes 69,000 training samples. PU1K is a new point cloud upsampling dataset introduced in PU-GCN. Overall, PU1K consists of 1,147 3D models, split into 1,020 training samples and 127 testing samples. The training set includes 120 3D models from the PU-GAN dataset [16] and 900 different models collected from ShapeNetCore [6]. The test set contains 27 models from PU-GAN and over 100 models from ShapeNetCore, covering 50 object categories.

The original PU1K dataset was modified to fit the patch-based upsampling pipeline, with training data generated through Poisson disk sampling from patches of 3D meshes. Specifically, the original training data comprises 69,000 samples, each containing 256 input points (low resolution) and 1,024 points ($4\times$ high resolution). To match the input model with the number of patches and AS inputs [26], we constrained PU1K to 8,192 points via Poisson disk sampling. Each model was divided into eight different local parts using patches and eight uniform subdivisions with AS to maintain model shape integrity. Similar to previous state-of-the-art point cloud upsampling models, each sample contains 256 input points (low resolution) and 1,024 points ($4\times$ high resolution). Under these conditions, our training data includes 16,320 samples.

4.1.2. Evaluation Metrics

To evaluate our point cloud upsampling network, we used three key metrics: Chamfer Distance (CD), Hausdorff Distance (HD), and Point-to-Surface Distance (P2F).

- CD assesses geometric accuracy through the mean nearest-neighbor distance.
- HD focuses on the maximum distance mismatch, highlighting extreme cases.

- P2F examines the proximity of upsampled points to the reference model’s surface, reflecting detail fidelity.

Our study inputs all N points in the point cloud. Next, trained model to upscale the seed patches and uniform segments by a scale factor of r . The farthest point sampling algorithm [9] will be used to combine all upsampled patches into a dense output point cloud with rN points. In the $4\times$ up-sampling experiments, we performed three low-to-high-resolution sampling conversions. Each test sample has a low-resolution point cloud with 256, 512, and 2,048 points and a high-resolution point cloud with 1,024, 2,048, and 8,196 points.

4.1.3. Comparison Methods

To verify the effectiveness of our proposed point cloud upsampling method, we compared it with several advanced algorithms: MPU [14], PU-GCN [15], Dis-PU [27], and PUCRN [28]. We also compared these algorithms with the ReLPU network using the same training pipeline.

For a fair and objective comparison, we obtained the open-source codes of these methods and trained and tested them on our computing equipment and training framework with identical parameter settings to establish the baseline.

4.1.4. Implementation Details

Our network was developed using the PyTorch framework and ran on an Ubuntu 22.04 system. We used an NVIDIA L20 GPU with 48GB of graphics memory and an Intel(R) Xeon(R) Platinum 8457C host with 100GB of RAM. The network was trained over 100 epochs with a batch size of 32. The initial learning rate was set to 0.0005, with a decay rate of 0.05.

4.2. Upsampling Results

In accuracy analysis, as mentioned above, we extensively evaluated the generalization performance of our network on the PU1K synthetic dataset, focusing on the differences between the original backbone network and the ReLPU pipeline incorporating both local and global features. The quantitative results for the PU1K dataset [15] in Table 1 show that our method performs consistently across different input scales (256, 512, 2,048 points) and outperforms the original network in CD, HD, and P2F metrics.

Methods	512 input points			2048 input points		
	CD↓	HD↓	P2F↓	CD↓	HD↓	P2F↓
MPU [14]	4.973	48.403	29.357	1.217	29.283	15.823
PU-GCN [15]	4.142	43.529	21.035	0.987	23.812	10.291
Dis-PU [27]	4.120	41.665	20.578	1.025	18.238	8.189
PUCRN [28]	3.605 ↓	35.778	15.246	0.918	13.870	6.633
ReLPU (MPU)	4.528	45.769	25.894	1.128	25.364	13.086
ReLPU (PU-GCN)	4.002	39.527	19.529	0.953	20.533	8.317
ReLPU (Dis-PU)	3.934	39.471	19.170	0.985	17.298	7.744
ReLPU (PUCRN)	3.625	34.873 ↓	14.802 ↓	0.910 ↓	13.117 ↓	5.682 ↓

Table 1: Performance comparison of different methods with ReLPU across input scales. Among them, the unit is 10^{-3} .

This result demonstrates the effectiveness of ReLPU, showcasing its superior capability in minimizing nearest-neighbor distance differences and reducing maximum point-to-point distance errors. Additionally, our method achieves low point-to-surface differences, which is crucial for maintaining topological consistency and mesh reconstruction from point clouds. However, compared to PUCRN [25], applying ReLPU to PUCRN yields slight differences in CD, HD, and P2F across the three input scales. This is related to PUCRN’s sequential three-stage refinement, which minimizes local and global discrepancies, as detailed in Section 4.4.

4.3. Noise Robustness Test

It is necessary to verify our model’s robustness to noise. Specifically, we tested the pre-trained model by adding random noise to sparse input data, with Gaussian noise satisfying a normal distribution $\mathcal{N}(0, 1)$ and scaled by a coefficient. We experimented at two noise levels: $\beta = 1\%$ and $\beta = 2\%$. Table 2 quantitatively compares the results of our model and state-of-the-art methods under different noise levels. In most test cases with noise, our proposed ReLPU outperformed the base models MPU [14], PU-GCN [15], Dis-PU [27], and PUCRN [28] showed robustness in CD and HD metrics.

4.4. Ablation Study

To verify the effectiveness of ReLPU compared to the original models, we visualized saliency maps in ReLPU across four models. To better understand our saliency maps, several maps are visualized in Figure 4, where we

Methods	$\beta = 1\%$		$\beta = 2\%$	
	CD↓	HD↓	CD↓	HD↓
MPU [14]	5.632	51.334	1.634	34.030
PU-GCN [15]	4.588	44.628	1.329	28.652
Dis-PU [27]	4.272	42.107	1.305	26.174
PUCRN [28]	3.610 ↓	37.086	1.276	17.502
ReLPU (MPU)	4.959	49.211	1.535	33.756
ReLPU (PU-GCN)	4.127	43.692	1.268	27.221
ReLPU (Dis-PU)	4.080	41.824	1.231	25.553
ReLPU (PUCRN)	3.617	36.253 ↓	1.180 ↓	16.948 ↓

Table 2: Robustness of models tested on PU1K with random noise, where noise follows a normal distribution $\mathcal{N}(0, 1)$, and β is the noise level. Among them, the unit is 10^{-3} .

Methods	ReLPU-			ReLPU		
	CD↓	HD↓	P2F↓	CD↓	HD↓	P2F↓
MPU [14]	1.185	27.830	15.072	1.128	25.364	13.086
PU-GCN [15]	0.974	22.516	9.851	0.953	20.533	8.317
Dis-PU [27]	0.979	18.001	7.969	0.985	17.298	7.744
PUCRN [28]	0.912	13.509	5.863	0.910 ↓	13.117 ↓	5.682 ↓

Table 3: Performance comparison of ReLPU- and ReLPU methods in 2048 input to 8192 scales. Among them, the unit is 10^{-3} .

color-code points based on their saliency score ranks, with higher numbers indicating higher saliency scores. We can see that the four models MPU [14], PU-GCN [15], Dis-PU [27], and PUCRN [28] have higher eigenvalues under patch input, especially at the edge curves. However, the global feature input based on AS input does not have particularly prominent feature values across the entire model. ReLPU, on the other hand, reflects its combination of the characteristics of both in terms of feature value contribution.

We compared ReLPU- and ReLPU to demonstrate the effectiveness of parallel feature processing over sequential processing. Results are shown in the Table 3. It can be seen that ReLPU based on parallel local and global inputs performs better than ReLPU based on sequential networks, which fully demonstrates the importance of parallel local and global feature fusion.

4.5. Visualization

Figure 5 provides a qualitative analysis on the PU1K dataset [15], demonstrating the effectiveness of our method in preserving overall shape, contour boundaries, and topological features, particularly in the zoomed-in areas. This is critical for applications that require surface reconstruction with high fidelity and topological accuracy. It can be seen that ReLPU can maintain the global structure of the point cloud model while being more detailed and accurate in the details of local features.

In the Figure 6, 2,048 sparse points are used as input, generating a dense point cloud with 8,192 points at a $4\times$ upsampling ratio. It shows the corresponding 3D mesh reconstructed using the Ball Pivoting algorithm [47]. From the reconstruction results, although MPU [14], PU-GCN [15], and Dis-PU [27] achieved state-of-the-art (SOTA) performance, they tend to overfit and produce holes when processing sparse boundaries of real-world objects. The results indicate that our method significantly improves overfitting in handling sparse and boundary regions. Our method not only enhances the uniformity and detail of point clouds but also substantially improves the accuracy of reconstructing holes and sparse regions, demonstrating the utility of our comprehensive approach in maintaining topological consistency while processing both local and global information.

5. Discussion

With the rapid advancement of deep learning, numerous novel architectures have emerged, such as Transformer [38], Mamba[48], RWKV[49], and xLSTM[50]. These methods have also inspired the development of hybrid approaches, combining their strengths with Graph Neural Networks (GNNs), resulting in architectures like Graph-Transformer[51], Graph-RWKV[52] and Graph-Mamba[53]. Moreover, there have been attempts to apply these new architectures to point cloud upsampling, exemplified by MBPU[54], which integrates Mamba into this domain.

Our approach ensures that future innovations in backbone architectures, such as those based on Transformer, Mamba, or other emerging models, can be seamlessly integrated into ReLPU. This adaptability not only future-proofs the framework but also ensures its relevance as point cloud processing techniques continue to evolve. The saliency map reflects the shape of the input data, as well as the local and global shapes, and can indeed represent local and global features, thus achieving the extraction of both types of features

in conjunction with the encoder at the input end. Through comprehensive experiments and analyses, we demonstrated the effectiveness of ReLPU in achieving superior geometric fidelity and robustness compared to state-of-the-art methods, making it a promising solution for point cloud upsampling in the era of rapidly evolving deep learning architectures.

6. Conclusion

In this research, we proposed the ReLPU framework to address the challenge of adapting to the rapid evolution of network structures while ensuring superior performance in point cloud upsampling. ReLPU was designed to be a flexible and adaptable framework that allows the backbone network to be easily replaced with advanced architectures. By enabling the parallel extraction of global and local features, ReLPU significantly enhances the quality and fidelity of upsampled point clouds.

The ReLPU framework for point cloud upsampling, integrating parallel global and local feature extraction. By employing identical autoencoders for both global and local inputs, our method effectively addresses challenges related to sparsity, noise, and topological inconsistencies. Extensive experiments on the PU1K and PU-GAN datasets demonstrated the superiority of ReLPU over state-of-the-art models in terms of geometric fidelity and robustness. Saliency map analysis further validated the importance of combining global and local features for accurate upsampling. The ReLPU framework not only improves the uniformity and detail of point clouds but also enhances its adaptability to real-world applications, making it a versatile solution for future advancements in point cloud processing.

7. Acknowledge

This research was supported by the National Natural Science Foundation of China under Grant 61773164.

References

- [1] W. Peng, Y. Wang, H. Zhang, Y. Cao, J. Zhao, Y. Jiang, Deep correspondence matching-based robust point cloud registration of profiled parts, *IEEE Transactions on Industrial Informatics* 20 (2) (2023) 2129–2143.

- [2] Z. Cai, N. Vasconcelos, Cascade r-cnn: Delving into high quality object detection, in: Proceedings of the IEEE conference on computer vision and pattern recognition, 2018, pp. 6154–6162.
- [3] X. Tang, K. Habashy, F. Huang, C. Li, D. Ban, Sca-net: Spatial and channel attention-based network for 3d point clouds, Computer Vision and Image Understanding 232 (2023) 103690.
- [4] T. Tan, J. M.-Y. Lim, J. J. Foo, R. Muniandy, 3d detection transformer: Set prediction of objects using point clouds, Computer Vision and Image Understanding 236 (2023) 103808.
- [5] J. Varley, C. DeChant, A. Richardson, J. Ruales, P. Allen, Shape completion enabled robotic grasping, in: 2017 IEEE/RSJ international conference on intelligent robots and systems (IROS), IEEE, 2017, pp. 2442–2447.
- [6] A. X. Chang, T. Funkhouser, L. Guibas, P. Hanrahan, Q. Huang, Z. Li, F. Yu, Shapenet: An information-rich 3d model repository, arXiv preprint arXiv:1512.03012 (2015).
- [7] Y. Xia, Y. Xia, W. Li, R. Song, K. Cao, U. Stilla, Asfm-net: Asymmetrical siamese feature matching network for point completion, in: Proceedings of the 29th ACM international conference on multimedia, 2021, pp. 1938–1947.
- [8] F. Scarselli, M. Gori, A. C. Tsoi, M. Hagenbuchner, G. Monfardini, The graph neural network model, IEEE transactions on neural networks 20 (1) (2008) 61–80.
- [9] C. R. Qi, H. Su, K. Mo, L. J. Guibas, Pointnet: Deep learning on point sets for 3d classification and segmentation, in: Proceedings of the IEEE conference on computer vision and pattern recognition, 2017, pp. 652–660.
- [10] W. Yuan, T. Khot, D. Held, C. Mertz, M. Hebert, Pcn: Point completion network, in: 2018 international conference on 3D vision (3DV), IEEE, 2018, pp. 728–737.

- [11] Y. Wang, Y. Sun, Z. Liu, S. E. Sarma, M. M. Bronstein, J. M. Solomon, Dynamic graph cnn for learning on point clouds, *ACM Transactions on Graphics (TOG)* 38 (5) (2019) 1–12.
- [12] L. Yu, X. Li, C. W. Fu, D. Cohen-Or, P. A. Heng, Pu-net: Point cloud upsampling network, in: *Proceedings of the IEEE conference on computer vision and pattern recognition*, 2018, pp. 2790–2799.
- [13] M. Henaff, J. Bruna, Y. LeCun, Deep convolutional networks on graph-structured data, *arXiv preprint arXiv:1506.05163* (2015).
- [14] W. Yifan, S. Wu, H. Huang, D. Cohen-Or, O. Sorkine-Hornung, Patch-based progressive 3d point set upsampling, in: *Proceedings of the IEEE/CVF Conference on Computer Vision and Pattern Recognition*, 2019, pp. 5958–5967.
- [15] G. Qian, A. Abualshour, G. Li, A. Thabet, B. Ghanem, Pu-gcn: Point cloud upsampling using graph convolutional networks, in: *Proceedings of the IEEE/CVF Conference on Computer Vision and Pattern Recognition*, 2021, pp. 11683–11692.
- [16] R. Li, X. Li, C. W. Fu, D. Cohen-Or, P. A. Heng, Pu-gan: a point cloud upsampling adversarial network, in: *Proceedings of the IEEE/CVF international conference on computer vision*, 2019, pp. 7203–7212.
- [17] I. Goodfellow, J. Pouget-Abadie, M. Mirza, B. Xu, D. Warde-Farley, S. Ozair, Y. Bengio, Generative adversarial networks, *Communications of the ACM* 63 (11) (2020) 139–144.
- [18] S. Qiu, S. Anwar, N. Barnes, Pu-transformer: Point cloud upsampling transformer, in: *Proceedings of the Asian conference on computer vision*, 2022, pp. 2475–2493.
- [19] W. Zhao, X. Liu, Z. Zhong, J. Jiang, W. Gao, G. Li, X. Ji, Self-supervised arbitrary-scale point clouds upsampling via implicit neural representation, in: *Proceedings of the IEEE/CVF Conference on Computer Vision and Pattern Recognition*, 2022, pp. 1999–2007.
- [20] Y. He, D. Tang, Y. Zhang, X. Xue, Y. Fu, Grad-pu: Arbitrary-scale point cloud upsampling via gradient descent with learned distance functions, in: *Proceedings of the IEEE/CVF Conference on Computer Vision and Pattern Recognition*, 2023, pp. 5354–5363.

- [21] D. Kim, M. Shin, J. Ryu, H. Lim, J. Paik, Pu-edgeformer++: An advanced hierarchical edge transformer for arbitrary-scale point cloud upsampling using distance fields, in: ICASSP 2024-2024 IEEE International Conference on Acoustics, Speech and Signal Processing (ICASSP), IEEE, 2024, pp. 6230–6234.
- [22] Y. Liu, B. Fan, S. Xiang, C. Pan, Relation-shape convolutional neural network for point cloud analysis, in: Proceedings of the IEEE/CVF conference on computer vision and pattern recognition, 2019, pp. 8895–8904.
- [23] Y. Zhou, O. Tuzel, Voxelnet: End-to-end learning for point cloud based 3d object detection, in: Proceedings of the IEEE conference on computer vision and pattern recognition, 2018, pp. 4490–4499.
- [24] B. Han, L. Deng, Y. Zheng, S. Ren, S3u-pvnet: Arbitrary-scale point cloud upsampling via point-voxel network based on siamese self-supervised learning, *Computer Vision and Image Understanding* 239 (2024) 103890.
- [25] W. Zhang, Q. Yan, C. Xiao, Detail preserved point cloud completion via separated feature aggregation, in: *Computer Vision–ECCV 2020: 16th European Conference, Glasgow, UK, August 23–28, 2020, Proceedings, Part XXV 16*, Springer International Publishing, 2020, pp. 512–528.
- [26] T. Zhang, Rethinking data input for point cloud upsampling, *arXiv preprint arXiv:2407.04476* (2024).
- [27] R. Li, X. Li, P. A. Heng, C. W. Fu, Point cloud upsampling via disentangled refinement, in: Proceedings of the IEEE/CVF conference on computer vision and pattern recognition, 2021, pp. 344–353.
- [28] H. Du, X. Yan, J. Wang, D. Xie, S. Pu, Point cloud upsampling via cascaded refinement network, in: Proceedings of the Asian Conference on Computer Vision, 2022, pp. 586–601.
- [29] Y. Zhu, Z. Zhang, X. Cheng, J. Zhang, Bilevel fusion with local and global cues for point cloud upsampling, *IEEE Transactions on Industrial Informatics* (2024).

- [30] L. Zhao, M. Shang, F. Gao, R. Li, F. Huang, J. Yu, Representation learning of image composition for aesthetic prediction, *Computer Vision and Image Understanding* 199 (2020) 103024.
- [31] C. R. Qi, L. Yi, H. Su, L. J. Guibas, Pointnet++: Deep hierarchical feature learning on point sets in a metric space, in: *Advances in neural information processing systems*, Vol. 30, 2017.
- [32] H. Su, S. Maji, E. Kalogerakis, E. Learned-Miller, Multi-view convolutional neural networks for 3d shape recognition, in: *Proceedings of the IEEE international conference on computer vision*, 2015, pp. 945–953.
- [33] F. J. Lawin, M. Danelljan, P. Tosteberg, G. Bhat, F. S. Khan, M. Felsberg, Deep projective 3d semantic segmentation, in: *Computer Analysis of Images and Patterns: 17th International Conference, CAIP 2017, Ystad, Sweden, August 22-24, 2017, Proceedings, Part I 17*, Springer International Publishing, 2017, pp. 95–107.
- [34] B. Graham, M. Engelcke, L. Van Der Maaten, 3d semantic segmentation with submanifold sparse convolutional networks, in: *Proceedings of the IEEE conference on computer vision and pattern recognition*, 2018, pp. 9224–9232.
- [35] Y. Guo, H. Wang, Q. Hu, H. Liu, L. Liu, M. Bennamoun, Deep learning for 3d point clouds: A survey, *IEEE Transactions on Pattern Analysis and Machine Intelligence* 43 (12) (2020) 4338–4364.
- [36] Y. Li, R. Bu, M. Sun, W. Wu, X. Di, B. Chen, Pointcnn: Convolution on x-transformed points, in: *Advances in neural information processing systems*, Vol. 31, 2018.
- [37] S. Shi, X. Wang, H. Li, Pointcnn: 3d object proposal generation and detection from point cloud, in: *Proceedings of the IEEE/CVF conference on computer vision and pattern recognition*, 2019, pp. 770–779.
- [38] A. Vaswani, Attention is all you need, in: *Advances in Neural Information Processing Systems*, Vol. 30, 2017.
- [39] H. Zhao, L. Jiang, J. Jia, P. H. Torr, V. Koltun, Point transformer, in: *Proceedings of the IEEE/CVF international conference on computer vision*, 2021, pp. 16259–16268.

- [40] S. Gurusurthy, S. Agrawal, High fidelity semantic shape completion for point clouds using latent optimization, in: 2019 IEEE Winter Conference on Applications of Computer Vision (WACV), IEEE, 2019, pp. 1099–1108.
- [41] X. Wen, T. Li, Z. Han, Y. S. Liu, Point cloud completion by skip-attention network with hierarchical folding, in: Proceedings of the IEEE/CVF conference on computer vision and pattern recognition, 2020, pp. 1939–1948.
- [42] L. Luo, L. Tang, W. Zhou, S. Wang, Z. X. Yang, Pu-eva: An edge-vector based approximation solution for flexible-scale point cloud upsampling, in: Proceedings of the IEEE/CVF International Conference on Computer Vision, 2021, pp. 16208–16217.
- [43] K. Simonyan, Deep inside convolutional networks: Visualising image classification models and saliency maps, arXiv preprint arXiv:1312.6034 (2013).
- [44] T. Zheng, C. Chen, J. Yuan, B. Li, K. Ren, Pointcloud saliency maps, in: Proceedings of the IEEE/CVF international conference on computer vision, 2019, pp. 1598–1606.
- [45] C. Ziwen, W. Wu, Z. Qi, L. Fuxin, Visualizing point cloud classifiers by curvature smoothing, arXiv preprint arXiv:1911.10415 (2019).
- [46] D. Schinagl, G. Krispel, H. Possegger, P. M. Roth, H. Bischof, Occam’s laser: Occlusion-based attribution maps for 3d object detectors on lidar data, in: Proceedings of the IEEE/CVF Conference on Computer Vision and Pattern Recognition, 2022, pp. 1141–1150.
- [47] F. Bernardini, J. Mittleman, H. Rushmeier, C. Silva, G. Taubin, The ball-pivoting algorithm for surface reconstruction, IEEE Transactions on Visualization and Computer Graphics 5 (4) (1999) 349–359.
- [48] A. Gu, T. Dao, Mamba: Linear-time sequence modeling with selective state spaces, arXiv preprint arXiv:2312.00752 (2023).
- [49] B. Peng, E. Alcaide, Q. Anthony, A. Albalak, S. Arcadinho, S. Biderman, H. Cao, X. Cheng, M. Chung, M. Grella, et al., Rwkv: Reinventing rnns for the transformer era, arXiv preprint arXiv:2305.13048 (2023).

- [50] M. Beck, K. Pöppel, M. Spanring, A. Auer, O. Prudnikova, M. Kopp, G. Klambauer, J. Brandstetter, S. Hochreiter, xlstm: Extended long short-term memory, arXiv preprint arXiv:2405.04517 (2024).
- [51] E. Min, R. Chen, Y. Bian, T. Xu, K. Zhao, W. Huang, P. Zhao, J. Huang, S. Ananiadou, Y. Rong, Transformer for graphs: An overview from architecture perspective, arXiv preprint arXiv:2202.08455 (2022).
- [52] Q. He, J. Zhang, J. Peng, H. He, X. Li, Y. Wang, C. Wang, Pointrwkv: Efficient rwkv-like model for hierarchical point cloud learning, arXiv preprint arXiv:2405.15214 (2024).
- [53] C. Wang, O. Tsepa, J. Ma, B. Wang, Graph-mamba: Towards long-range graph sequence modeling with selective state spaces, arXiv preprint arXiv:2402.00789 (2024).
- [54] J. Song, W. Yang, Z. Li, W.-M. Chen, B. Fei, Mbpv: A plug-and-play state space model for point cloud upsampling with fast point rendering, arXiv preprint arXiv:2410.15941 (2024).

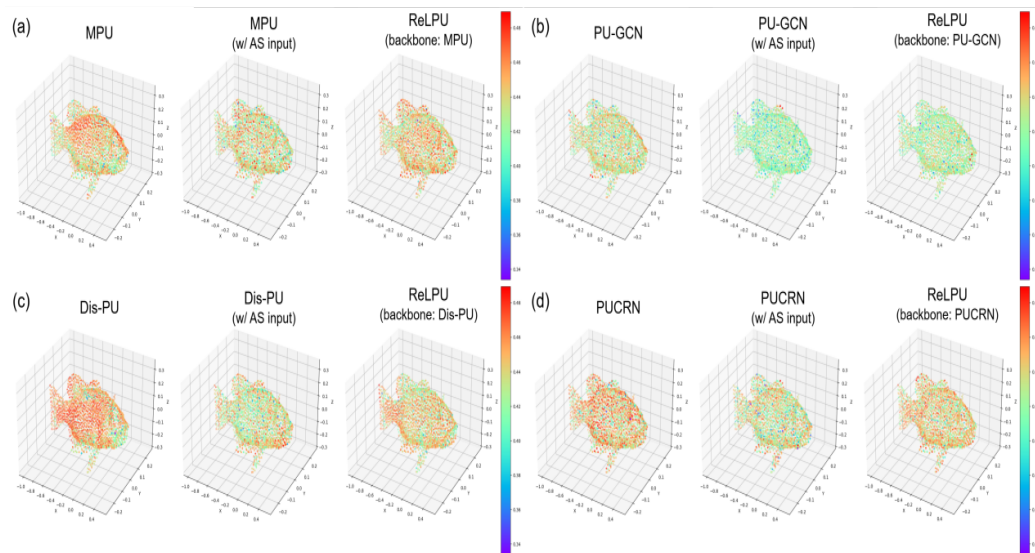
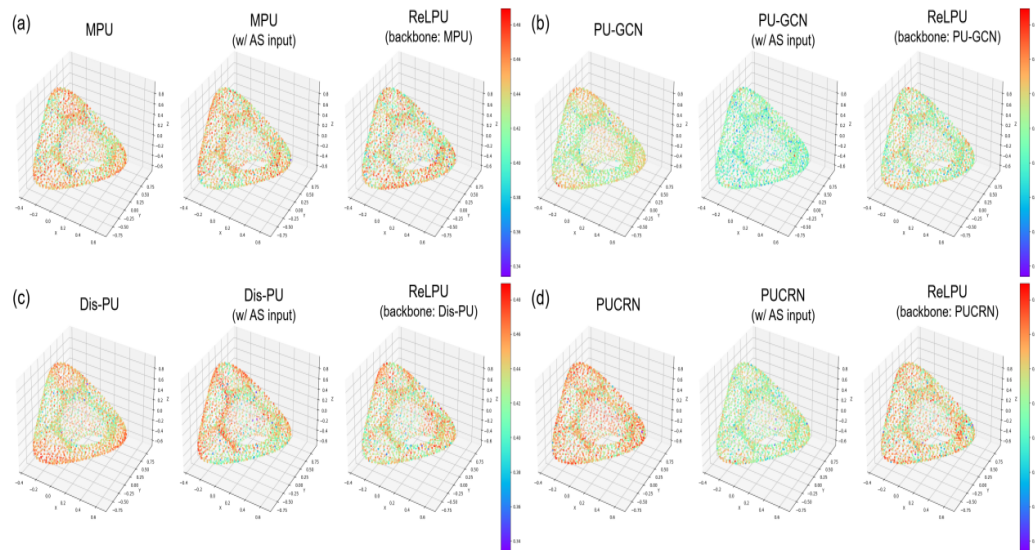


Figure 4: Visualizes saliency maps comparing ReLPU and original models (MPU, Dis-PU, PU-GCN, PUCRN) by patch (local) inputs and AS (global) inputs. Points are color-coded based on saliency score ranks, where higher values represent higher saliency.

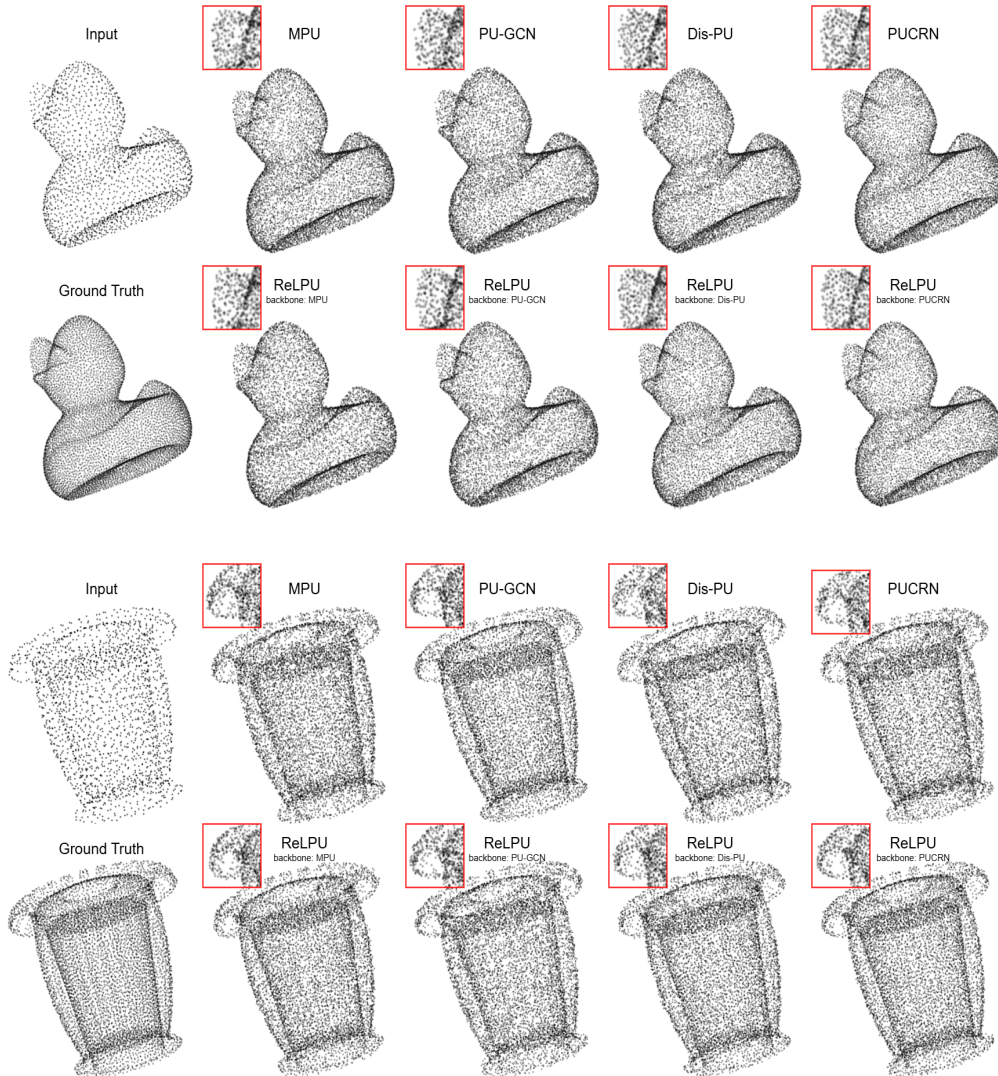


Figure 5: Comparisons to state-of-the-art methods (MPU, PU-GCN, Dis PU and PUCRN) with ReLPU in ($4\times$) upsampling synthetic point cloud data using 2048 input points.

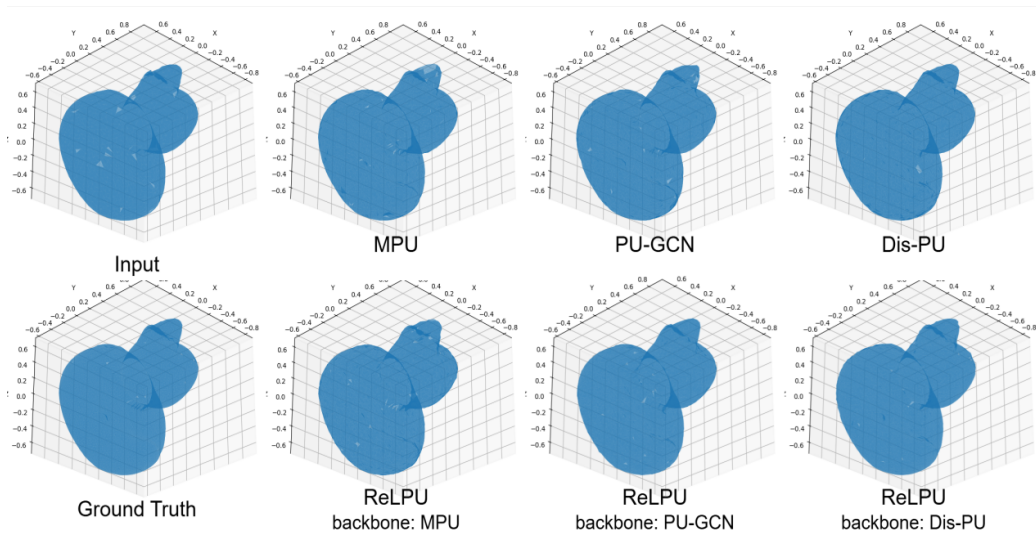
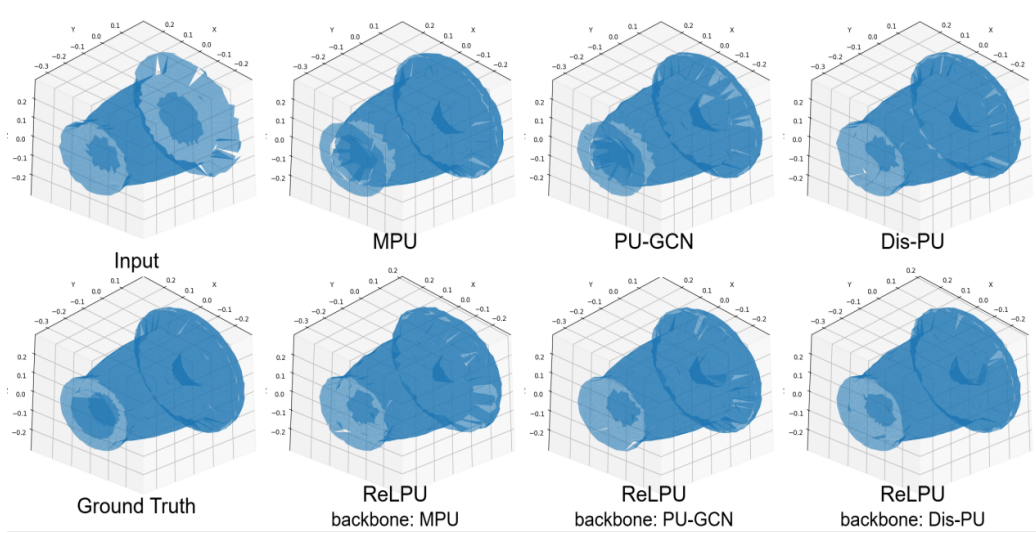


Figure 6: Reconstruct the mesh from point cloud after upsampling by using BallPivoting [47] algorithm. Our method can be less holes.